

KRADA: Known-region-aware Domain Alignment for Open World Semantic Segmentation

Chenhong Zhou^{*1}, Feng Liu^{*2}, Chen Gong³, Tongliang Liu⁴, Bo Han¹, and William Cheung¹

¹Hong Kong Baptist University

²DeSI Lab, AAII, University of Technology Sydney

³Key Laboratory of Intelligent Perception and Systems for High-Dimensional Information of MoE, Nanjing University of Science and Technology

⁴TML Lab, University of Sydney

Abstract

In *semantic segmentation*, we aim to train a pixel-level classifier to assign category labels to *all* pixels in an image, where labeled training images and unlabeled test images are from the *same distribution* and share the *same label set*. However, in an open world, the unlabeled test images probably contain *unknown categories* and have *different distributions* from the labeled images. Hence, in this paper, we consider a new, more realistic, and more challenging problem setting where the pixel-level classifier has to be trained with labeled images and unlabeled open-world images—we name it *open world semantic segmentation* (OSS). In OSS, the trained classifier is expected to identify unknown-class pixels and classify known-class pixels well. To solve OSS, we first investigate which distribution that unknown-class pixels obey. Then, motivated by the goodness-of-fit test, we use *statistical measurements* to show how a pixel *fits* the distribution of an unknown class and select highly-fitted pixels to form the *unknown region* in each image. Eventually, we propose an end-to-end learning framework, *known-region-aware domain alignment* (KRADA), to distinguish unknown classes while aligning distributions of known classes in labeled and unlabeled open-world images. The effectiveness of KRADA has been verified on two synthetic tasks and one COVID-19 segmentation task.

1 Introduction

Semantic segmentation aims to assign one category label to each pixel in an image, which has a large variety of applications from autonomous driving [1, 2], indoor navigation [3] to medical image analysis [4]. In recent years, deep learning-based methods have been developing rapidly and achieved remarkable successes in semantic segmentation [5]. These methods usually train a *deep convolutional neural network* (DCNN) using a training set that contains pairs of images and pixel-level labels [6] to segment unlabeled test images. These works commonly assume that the training images and test images are taken from *the same scenario* and share *the same category label set* [7, 8].

However, in an open world, test images might be taken from a different scenario and have additional category labels compared to training images. For example, in autonomous driving, to reduce the great demand for accurately annotated images, a synthetic dataset, such as SYNTHIA [9], is commonly used to train a network for segmentation of urban scenes. Unfortunately, a realistic urban scenario is quite complex and different from the simulated one. Thus, real-world urban images probably contain some additional category labels (i.e., *unknown classes*) that are not present in the synthetic images.

^{*}Equal contribution.

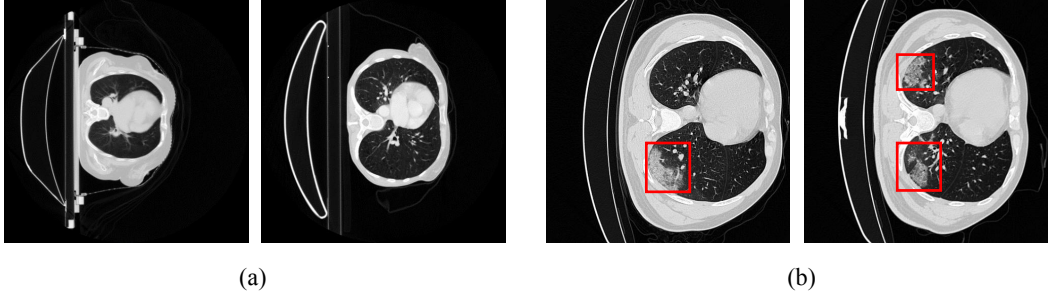


Figure 1: Illustration of the differences in two CT datasets. (a) Examples of normal CT scans. (b) Examples of COVID-19 CT scans, where the infected area is circled by red boxes. These two datasets vary at the visual level (domain shift) and are not consistent at the semantic level (category shift).

Another representative example is *Coronavirus Disease 2019* (COVID-19) infection segmentation task. Due to scarce annotated images in COVID-19 datasets, existing chest *Computed Tomography* (CT) scans can be utilized as training images to assist COVID-19 segmentation. However, the segmentation models trained on a normal CT dataset usually show poor performance to segment the COVID-19 infected area, as a result of *domain shift* and *category shift* issues. *Domain shift* refers to a distributional discrepancy caused by the variations in light, conditions, and device types for the acquisition of training and test images, while *category shift* means the inconsistent label sets between training and test images, e.g., COVID-19, a new disease which has never appeared in the training images. Figure 1 illustrates both issues in the COVID-19 segmentation task.

Regarding such a realistic and challenging segmentation scenario, we name it *open world semantic segmentation* (OSS). Although *closed-set domain adaptation segmentation* (CSDAS) methods [10, 11, 12, 13, 14, 15, 16, 17, 18, 19] have been extensively studied to overcome the domain-shift issue, they are not applicable to OSS because they probably mistakenly align unknown target data (i.e., open-world images) with source data (i.e., training images), leading to negative transfer [20].

In this paper, to solve OSS, we first explore the inherent property of unknown classes and propose that the distribution of softmax outputs for an unknown class would conform to a uniform distribution. Motivated by the goodness-of-fit test, we propose to use *statistical measurements* to describe how likely a target pixel is an unknown pixel, i.e., how well the output probability distribution of a target pixel *fits* the distribution of an unknown class. The distribution disparity between these two distributions can be measured by statistical measurements. Here we adopt two statistical metrics: 1) Kullback–Leibler (KL) divergence, a general criterion for testing goodness of fit [21]; 2) Kolmogorov (or Uniform) metric, a test statistic used in the Kolmogorov-Smirnov goodness-of-fit test [22].

Based on these statistical measurements, we can identify the highly-fitted pixels as “unknown”, while the *unknown region* in a target image can be determined. Hence, a segmentation model can be trained using source data and pseudo-labeled target data to achieve a better domain alignment by rejecting unknown target regions and aligning the distributions only for known-class data. We call this framework *known-region-aware domain alignment* (KRADA), which is independent of the network architecture and can be easily realized on existing CSDAS methods to adapt them for OSS.

We have realized KRADA on three CSDAS methods in our experiments and evaluate them on two synthetic-to-real street scene segmentation tasks and one COVID-19 segmentation task. Experimental results show that KRADA enables CSDAS methods to identify unknown-class regions and achieve a better overall adaptation, verifying its effectiveness and good generalization ability.

2 Problem Setup: Open World Semantic Segmentation

We address the problem of open world semantic segmentation (OSS) that is defined as follows.

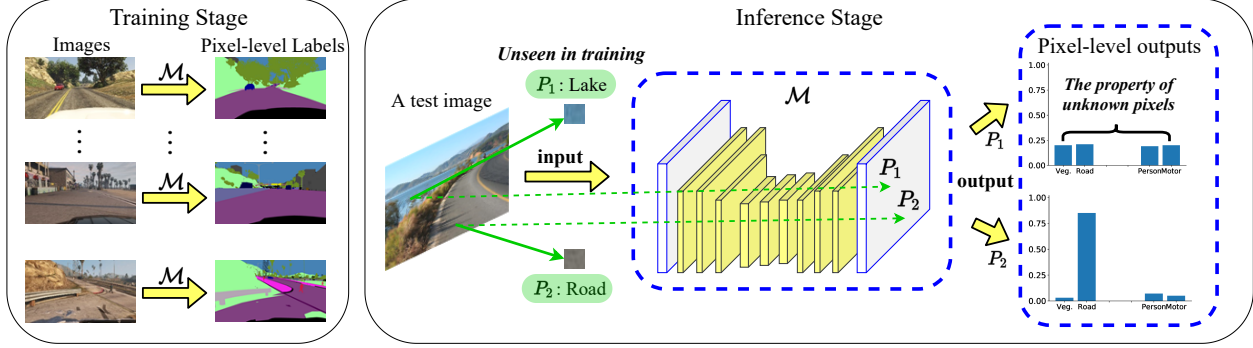


Figure 2: An illustration of the output distribution property of an unknown pixel. A test image contains a “lake” region whose semantic label (lake) is not present during training. The well-trained segmentation model \mathcal{M} *cannot* recognize such a “lake” pixel (P_1) and outputs a probability vector over known classes for it. Its probability distribution conforms to a uniform-like distribution, different from that of a known pixel (P_2).

Problem 1 (Open World Semantic Segmentation). *Let X^T be a m.r.v. defined on the space $\mathcal{X} = \mathbb{R}^{Ch \times H \times W}$ and follow a distribution $P(X^T)$, (X^S, Y^S) be a m.r.v. defined on the space $\mathcal{X} \times \mathcal{Y}$ and follow a distribution $Q(X^S, Y^S)$, where Ch , H , W are integers regarding the channel, height, and weight of an image, $\mathcal{Y} = \mathbb{L}^{H \times W}$ is a label space, and $\mathbb{L} = \{1, \dots, K\}$ is the category label set. In open world semantic segmentation (OSS), the category label set for X^T has an additional label $K + 1$ ¹ (i.e., category shift), and $Q_X(X^S)$ is different from $P(X^T)$ (i.e., domain shift). We aim to train a segmentation model $\mathcal{M} : \mathcal{X} \rightarrow \mathcal{Y}^T$ with observations from (X^S, Y^S) and X^T such that \mathcal{M} can accurately annotate each pixel in the observation from X^T , where $\mathcal{Y}^T = \{1, \dots, K, K + 1\}^{H \times W}$. Specifically, given an observation x^t from X^T , $\mathcal{M}(x^t) \in \{1, \dots, K + 1\}^{H \times W}$ can segment x^t to $K + 1$ classes well.*

Different from the open world setting in [23, 24] which entirely concentrates on unknown classes, our proposed setting further considers a common phenomenon in known classes that a distributional discrepancy exists, apart from detecting unknown classes. Moreover, some existing studies about open set segmentation [25, 26] also do not consider the distribution shift problem. Instead, we expect the segmentation model in OSS to solve both domain shift and category shift issues simultaneously.

3 How Do We Determine Unknown Pixels?

To solve OSS, the critical issue is how to separate unknown pixels from known pixels in target images. Due to lack of unknown-class supervision, a classifier trained with source data will forcibly label an unknown pixel as one of the known (source) classes [27]. To avoid this issue, we consider introducing unknown-class pseudo-labels into a segmentation model so that the model can be trained to learn unknown-class information from pseudo-labels and gain the ability to identify unknown pixels. Before the generation of unknown-class pseudo-labels, we need to know what property an unknown class has. In other words, what can we use to represent an unknown class? If given this property, we can exploit it to determine whether a pixel is unknown.

As unknown classes have never appeared in the training data, a well-trained model cannot recognize an unknown pixel and would output the most unbiased prediction probabilities (over known classes) for it. Hence, the output probability distribution for an unknown pixel would conform to a uniform distribution. Those target pixels that have this property would be considered unknown. We illustrate this property in Figure 2, where the output of a “lake” pixel (P_1) in a test image conforms to a uniform-like distribution, as this pixel is an unknown pixel for \mathcal{M} .

¹Note that the label $K + 1$ represents all categories that do not appear in \mathbb{L} , i.e., the unknown class.

4 A General Framework to Solve OSS

Generally, a segmentation network \mathcal{M} consists of a feature extractor F and a pixel-level classifier C to encode input images into the feature space and map the features to the label space \mathcal{Y} defined in Problem 1, respectively. The network \mathcal{M} can be formalized as $\mathcal{M} = C \circ F$ and it is usually trained with labeled source data:

$$L_{seg}^S = \hat{\mathbb{E}}[\ell(C(F(X^S)), Y^S)], \quad (1)$$

where $\mathbb{E}[\cdot]$ denotes the expectation over m.r.v.s, $\hat{\mathbb{E}}[\cdot]$ is the empirical estimation of $\mathbb{E}[\cdot]$, and $\ell(\cdot, \cdot)$ is a *cross-entropy* (CE) loss function. In OSS, an open-set pixel-level classifier C is expected to output an image defined on \mathcal{Y}^T to identify unknown target pixels and classify known-class pixels well. However, the known-class supervision L_{seg}^S is not sufficient to achieve this. Thus, we consider adding auxiliary supervision L_{seg}^T by introducing *unknown-class pseudo-labels* into the training stage:

$$L_{seg} = L_{seg}^S + \alpha L_{seg}^T, \quad (2)$$

where

$$L_{seg}^T = \hat{\mathbb{E}}[\ell(C(F(X^T)), \hat{Y}^T)], \quad (3)$$

and \hat{Y}^T denotes the unknown-class pseudo-labels of target data, and α is a hyperparameter to control the loss weight of unknown classes. Consequently, C can be trained using the labeled source and pseudo-labeled target data. We introduce the generation of unknown-class pseudo-labels as follows.

4.1 Unknown-class Pseudo-label Generation

Based on the distribution property of unknown classes, we consider determining whether a target pixel is unknown from a statistical point of view. Specifically, goodness-of-fit tests indicate the goodness of fit of a model by comparing the observed data with the data expected under the model [28, 29]. Motivated by this, we utilize statistical measurements to measure how well the output probability distribution for a target pixel fits a uniform distribution. Then, those highly-fitted target pixels would be labeled as unknown pixels.

In this paper, we adopt Kullback–Leibler (KL) divergence, a criterion used in goodness-of-fit tests [21], to measure the distribution disparity between output probability distribution and a uniform distribution. KL divergence is a non-symmetric measure that quantifies how much one distribution differs from another one, indicating the information lost when $q(x)$ is used to approximate $p(x)$:

$$D_{KL}(p(x) || q(x)) = \sum_{x \in X} p(x) \log\left(\frac{p(x)}{q(x)}\right). \quad (4)$$

Remark 1. *Typically, $p(x)$ represents a "true" distribution or a theoretical distribution while $q(x)$ represents the observed distribution. Here $p(x)$ is a uniform distribution, and $q(x)$ is the prediction probability outputted by a model for a target pixel. Other statistical metrics can be chosen, and more available metrics are offered in [22].*

To obtain the prediction probability over known classes (i.e., $q(x)$ in Eq. (4)), we additionally introduce a pixel-level known-class classifier C^* to output an image defined on \mathcal{Y} . C^* can be supervised by minimizing the segmentation loss on the source data:

$$L_{seg}^* = L_{seg}^{S,*} = \hat{\mathbb{E}}[\ell(C^*(F(X^S)), Y^S)]. \quad (5)$$

For a target image $x^t \in X^T$, C^* aims to produce a probability map $p^{t,*}$ of shape $K \times H \times W$:

$$p^{t,*} = \text{softmax}(C^*(F(x^t))). \quad (6)$$

More specifically, $p_{ij}^{t,*} \in \mathbb{R}^K$ implies the probability vector for a pixel $\{i, j\}$ in x^t , and thus $\sum_{c \in \mathbb{L}} p_{ij}^{t,c} = 1$. Here $p^u = [\frac{1}{K}, \dots, \frac{1}{K}] \in \mathbb{R}^K$ is used to denote a uniform distribution. Hence, we can calculate the distributional

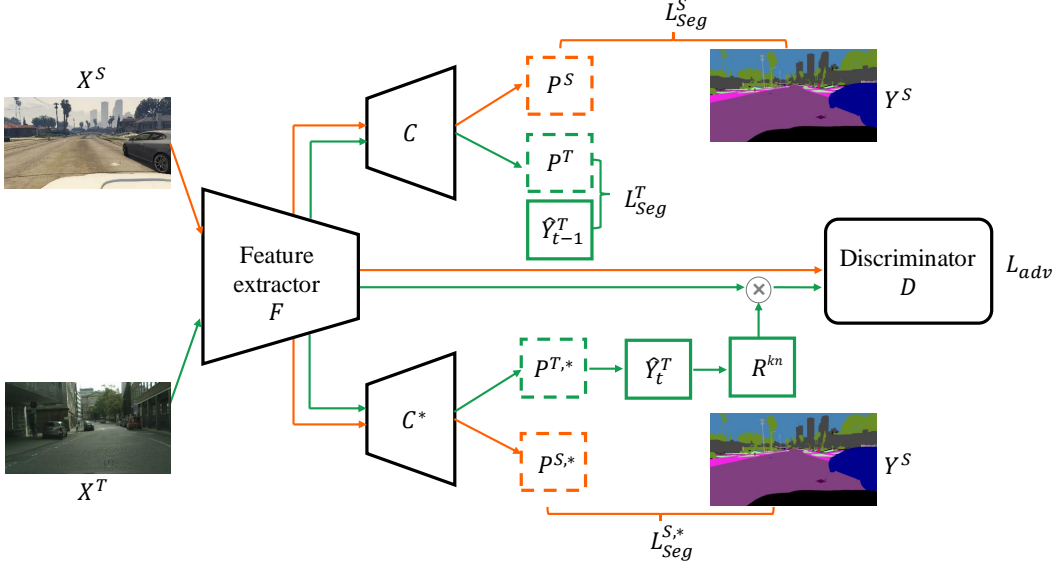


Figure 3: Overview of the proposed KRADA realized on the existing CSDAS methods. It consists of a feature extractor (F), a pixel-level classifier (C), a known-class classifier (C^*), and a discriminator (D). The orange and green parts denote the source domain flow and target domain flow, respectively. Specifically, C is optimized under the supervision from both source domain and pseudo-labeled target domain, where \hat{Y}_{t-1}^T denotes the pseudo-labels of target data previously produced at last time ($t-1$). The aim of C^* is to generate the new pseudo-labels \hat{Y}_t^T at time (t) and known-class region R^{kn} . Then we forward the features of source images and known regions in target images into D to perform known-class-aware domain alignment.

divergence between $p_{ij}^{t,*}$ and p^u for each target pixel and compare it with a threshold δ . Those target pixels whose distribution is close to a uniform distribution are marked as unknown, which can be formalized as:

$$\hat{y}_{ij}^{t,K+1} = \begin{cases} 1, & \text{if } D_{KL}(p^u || p_{ij}^{t,*}) < \delta, \\ 0, & \text{otherwise,} \end{cases} \quad (7)$$

where KL divergence can be replaced with Kolmogorov metric or other probability metrics in [22].

Remark 2. Note that \hat{y}^t is initially a $(K+1) \times H \times W$ shaped tensor with all elements equaling to zero. $\hat{y}_{ij}^t \in \mathbb{R}^{K+1}$ is a one-hot vector for a target pixel. If $\hat{y}_{ij}^{t,K+1}$ equals to one, it means that this pixel will be pseudo-labeled as unknown; otherwise, this pixel remains unlabeled.

Eventually, we can produce pseudo-labels \hat{Y}^T for target images X^T . Particularly, pseudo-labels are constantly updated when target images are fed into the network once again. As a consequence, the network can be optimized using source data and previously pseudo-labeled target data while generating new pseudo-labels, which is different from the multi-round training mechanism in [16, 17, 30] that alternatively optimizes pseudo-label generation and network training.

Remark 3. It should be emphasized that here KL divergence is not equivalent to entropy since entropy measures prediction uncertainty and only depicts the internal relationships of known classes for a target pixel. It does not exploit the property of unknown classes, so it does not measure the distance of a pixel to an unknown class in a strict sense. This is confirmed by the fact that those pixels with high entropy are probably the boundary pixels, not unknown pixels.

4.2 Known-region-aware Domain Alignment (KRADA)

Since there is a domain shift between source and target domains, we also consider reducing this domain gap when minimizing Eq. (2). Adversarial training (AT) based methods are a predominant stream of minimizing domain gap, e.g., existing CSDAS works. These methods train \mathcal{M} to learn domain-invariant features by confusing a domain discriminator D . An adversarial loss is minimized to align the distributions between source and target domains at input level [31, 32], feature level [10, 11, 33, 14, 31], or output level [13, 15, 12]. The main difference between these three kinds of domain alignment is the input of the discriminator D . For a clear illustration, we take the feature-level alignment as an example in the following. In this case, the input of D is the source features or target features produced by F , and the adversarial loss is formulated as:

$$L_{adv}^{AT} = -\hat{\mathbb{E}} [\log(D(F(X^S)))] - \hat{\mathbb{E}} [\log(1 - D(F(X^T)))] . \quad (8)$$

Unfortunately, these CSDAS works cannot be directly applied to OSS since they would forcefully match the feature distributions of two domains, which makes unknown target data mistakenly aligned with source data, leading to negative transfer.

To avoid this issue, we consider that cross-domain adaptation should be performed only on the known-class data. Therefore, a novel *known-region-aware domain alignment* (KRADA) is proposed to align the target image regions predicted as known with the source images, which is shown in Figure 3. The adversarial loss can be developed from Eq. (8) to:

$$L_{adv} = -\hat{\mathbb{E}} [\log(D(F(X^S)))] - \hat{\mathbb{E}} [\log(1 - D(F(X^T) \cdot R^{kn}))] , \quad (9)$$

where R^{kn} is a binary mask to denote the known-class region predicted for target images. Once pseudo-labels \hat{Y}^T are determined, R^{kn} can also be obtained by:

$$R_{ij}^{kn} = \begin{cases} 0, & \text{if } \hat{y}_{ij}^{t,K+1} = 1. \\ 1, & \text{otherwise.} \end{cases} \quad (10)$$

We multiply R^{kn} and each channel of target feature maps and then forward the features of known-class regions in target images into D . Eventually, unknown-class regions are rejected, and only the known regions of target images are aligned with source images. It is worth mentioning that KRADA does not have any requirement for the discriminator, so the alignment process of KRADA has no difference from that of original AT methods, except for the target inputs of the discriminator. This indicates that KRADA is *independent of* the model or structure and has good extensibility.

5 Realizations of KRADA on Existing CSDAS Methods

In this section, we realize the proposed KRADA on existing CSDAS methods, as illustrated in Figure 3. The original CSDAS network generally consists of a feature extractor (F), a pixel-level classifier (C), and a discriminator (D). To solve OSS, we additionally introduce a known-class classifier (C^*) which is arranged in parallel with C . The architecture of C^* is similar to that of C except for the last convolutional layer with K output channels. The training details are summarized in Algorithm 1. We use source data (X^S, Y^S) and target data X^T with previously generated pseudo-labels \hat{Y}_{t-1}^T to calculate L_{seg} according to Eqs. (1), (2), and (3) (line 2), where the initial pseudo-labels \hat{Y}_0^T is a tensor of $(K+1) \times H \times W$ with all elements being zero.

Then we use source data to calculate L_{seg}^* according to Eq. (5) (line 3). After generating the new pseudo-labels \hat{Y}_t^T and the known-region map R^{kn} according to Eqs. (6), (7), and (10) (line 4), we calculate L_{adv} according to Eq. (9) (line 5). These network parameters are updated until the network converges (lines 6-9). Finally, we obtain the segmentation results \tilde{Y}^T of target data (line 11). Overall, KRADA has no specific requirements for CSDAS architectures (F , C , and D) and can be easily integrated into CSDAS methods to form unified segmentation models. Therefore, a series of CSDAS methods can be adapted to solve OSS by a minor modification. In our experiments, we realize KRADA using *three* representative CSDAS methods, and the results show that KRADA can help address the OSS problem well.

Algorithm 1 An implementation of KRADA on existing CSDAS methods.

Input: source data (X^S, Y^S) , target data X^T , initial pseudo-labels \hat{Y}_0^T .
Parameter: pseudo-label parameters: δ, α , network parameters: $\theta_F, \theta_C, \theta_D, \theta_{C^*}$, the number of iteration N , learning rate: γ .
Output: predicted target labels: \tilde{Y}^T .

- 1: **for** $t = 1$ **to** N **do**
- 2: calculate L_{seg} using $(X^S, Y^S, X^T, \hat{Y}_{t-1}^T)$ according to Eq. (1), (2), and (3).
- 3: calculate L_{seg}^* using (X^S, Y^S) according to Eq. (5).
- 4: generate \hat{Y}_t^T, R^{kn} using X^T according to Eq. (6), (7), and (10).
- 5: calculate L_{adv} using (X^S, X^T, R^{kn}) according to Eq. (9).
- 6: $\theta_F = \theta_F - \gamma \nabla_{\theta_F} (L_{seg} + L_{seg}^* - L_{adv})$
- 7: $\theta_C = \theta_C - \gamma \nabla_{\theta_C} L_{seg}$
- 8: $\theta_D = \theta_D - \gamma \nabla_{\theta_D} L_{adv}$
- 9: $\theta_{C^*} = \theta_{C^*} - \gamma \nabla_{\theta_{C^*}} L_{seg}^*$
- 10: **end for**
- 11: Prediction: $\tilde{Y}^T \leftarrow C(F(X^T))$.

6 Experiments

Synthetic OSS tasks. Since the researches about OSS have not been explored, there is no public dataset for such a new setting. Based on two synthetic-to-real benchmark tasks in CSDAS: SYNTHIA [9] \rightarrow Cityscapes [1] and GTA5 [34] \rightarrow Cityscapes, we adjust these two tasks to simulate the OSS scenario. For the task SYNTHIA \rightarrow Cityscapes, we select three classes (wall, light, and bus) to form the unknown class and discard those images containing either of the three classes. The remaining images in SYNTHIA are regarded as the source domain. For the task GTA5 \rightarrow Cityscapes, we choose two classes (fence and sign) to form the unknown class. Those images which do not contain the unknown class in GTA5 are retained as the source domain. Following the common practice in CSDAS, we use the Cityscapes training set as the target domain and evaluate our models on the Cityscapes validation set with a widely adopted evaluation metric: mean Intersection over Union (mIoU) for all classes. Considering the evaluation protocol in unsupervised open set domain adaptation (UOSDA) [7, 8, 35], we also report the mIoU averaged over known classes only, denoted as mIoU* in this paper. To justify the generalization ability of KRADA, we implement KRADA on three CSDAS methods: 1) AdaptSegNet [12], 2) CLAN [13], and 3) a state-of-the-art adversarial training-based method—FADA [14], denoted as AdaptSegNet + KRADA, CLAN + KRADA, and FADA + KRADA, respectively. Additionally, OSBP [8] is used as the baseline, which is one of the few UOSDA methods that can be modified to segmentation tasks by simply convolutionalizing its network architecture. More data descriptions and implementation details are described in Appendix B.

Results on synthetic OSS tasks. We present the results of SYNTHIA \rightarrow Cityscapes in Table 1. Compared with Source-only², OSBP increases unknown-class IoU from 0.0% to around 2.0%. But this achievement is at the cost of the segmentation performance on known classes as both mIoU and mIoU* of OSBP significantly decrease. Compared to Source-only, AdaptSegNet, CLAN, and FADA promote the adaptation for known classes by a large margin, but their unknown-class IoU values are stable at 0.0%, which means that they cannot recognize the unknown class. After the realizations of KRADA, these three modified models consistently outperform OSBP with huge margins and achieve significant improvements in the segmentation of unknown regions. Moreover, these modified models achieve higher mIoU and mIoU* compared to their corresponding versions without KRADA. This is because KRADA mitigates negative transfer caused by unknown classes in the target domain wrongly matched to known classes in the source domain. Thus, the segmentation of known classes improves. Particularly, FADA + KRADA achieves the best performance at both best and last epochs.

Table 2 presents the results of GTA5 \rightarrow Cityscapes. We can see that KRADA enables three CSDAS models to consistently outperform OSBP and improve the unknown-class IoU from 0.0% to around 1.0%.

²Source-only refers to a base model only trained on source images without adaptation.

Table 1: Results on SYNTHIA → Cityscapes. “B” denotes the best score during training, while “L” denotes the last score at the end of training.

Method	road	side.	build.	fence	pole	sign	veg.	sky	person	rider	car	motor	bike	unk.	mIoU	mIoU*
Soure-only	B 39.9	19.2	65.4	0.0	22.4	2.0	63.8	70.2	47.8	14.0	47.9	7.5	26.2	0.0	30.4	32.8
	L 34.5	18.0	61.7	0.0	20.9	2.0	60.1	67.8	48.0	15.7	46.5	8.4	26.2	0.0	29.3	31.5
OSBP [8]	B 31.7	17.4	67.5	0.0	20.3	0.4	63.0	71.0	33.3	11.7	60.8	7.7	26.2	1.7	29.5	31.6
	L 28.7	16.3	66.6	0.1	19.5	0.6	59.0	72.7	28.9	7.0	50.2	3.2	23.9	2.0	27.0	29.0
AdaptSegNet [12]	B 72.4	35.7	75.6	0.0	14.6	1.1	69.9	75.5	37.7	14.4	70.6	12.2	29.9	0.0	36.4	39.2
	L 66.6	35.9	74.0	0.0	14.2	1.1	68.4	72.8	35.2	13.6	62.4	10.4	27.8	0.0	34.5	37.1
CLAN [13]	B 83.4	37.6	76.8	0.0	21.9	2.7	77.8	78.7	49.9	17.7	80.1	12.5	28.6	0.0	40.6	43.7
	L 82.9	38.1	76.1	0.0	21.7	2.3	77.1	77.0	47.5	17.1	78.5	10.7	26.8	0.0	39.7	42.8
FADA [14]	B 84.5	39.0	79.0	0.0	27.2	1.4	83.0	73.6	38.3	13.3	75.6	5.1	38.6	0.0	39.9	43.0
	L 82.6	37.5	79.0	0.0	25.8	1.8	82.9	74.8	37.7	12.9	76.3	6.6	35.0	0.0	39.5	42.5
AdaptSegNet + KRADA	B 65.2	34.1	75.6	0.0	18.7	0.7	74.5	75.8	48.8	16.1	74.7	8.8	33.9	1.8	37.8	40.5
	L 63.7	33.1	76.0	0.0	17.8	0.8	74.1	75.5	48.1	15.7	73.5	7.7	33.3	1.9	37.2	39.9
CLAN + KRADA	B 80.6	36.8	77.8	0.0	24.6	2.4	76.7	77.1	49.3	18.1	81.7	14.3	30.7	2.1	40.9	43.9
	L 77.6	37.4	77.0	0.0	22.4	2.0	76.2	75.2	48.5	17.3	80.1	13.8	29.8	1.6	39.9	42.9
FADA + KRADA	B 85.0	42.2	79.4	0.0	26.5	1.4	82.1	73.9	46.0	14.8	78.1	10.2	42.1	4.0	41.8	44.7
	L 82.2	39.4	79.2	0.0	29.0	1.5	82.1	75.9	44.9	13.9	78.5	8.9	38.5	3.3	41.2	44.2

Table 2: Results on GTA5 → Cityscapes. “B” denotes the best score during training, while “L” denotes the last score at the end of training.

Method	road	side.	build.	wall	pole	light	terrain	veg.	sky	person	rider	car	truck	bus	train	motor	bike	unk.	mIoU	mIoU*
Soure-only	B 80.0	6.8	74.4	16.2	25.6	27.9	77.2	15.7	72.5	52.4	19.5	70.5	16.2	17.1	0.9	11.0	0.3	0.0	32.5	34.4
	L 77.6	4.3	70.9	14.9	22.0	26.5	75.6	10.2	71.3	51.8	17.0	69.6	14.9	16.3	0.1	12.4	0.3	0.0	30.9	32.7
OSBP [8]	B 84.9	36.8	77.9	18.4	24.1	23.0	80.6	26.3	74.5	51.3	13.2	74.8	20.1	23.0	0.0	16.4	0.0	0.5	35.9	38.0
	L 85.7	35.7	78.0	15.6	23.8	20.6	79.6	29.8	70.5	51.0	11.9	72.6	18.4	19.1	0.0	16.6	0.0	0.2	35.0	37.0
AdaptSegNet [12]	B 78.3	14.4	77.9	14.4	25.6	34.3	80.2	18.3	82.9	56.0	25.0	76.5	14.7	3.8	0.5	27.9	0.9	0.0	35.1	37.2
	L 71.2	14.4	73.9	10.2	24.9	33.2	81.3	19.1	83.8	53.8	24.0	72.7	14.4	1.9	0.6	30.0	1.4	0.0	33.9	35.9
CLAN [13]	B 87.8	17.5	76.8	22.4	23.0	26.6	82.6	30.0	80.0	54.8	16.6	83.6	35.7	43.2	0.0	26.7	0.2	0.0	39.3	41.6
	L 87.2	16.7	76.0	19.9	21.7	27.3	82.5	28.4	79.2	55.0	9.3	83.1	32.2	38.0	0.0	26.8	0.2	0.0	38.0	40.2
FADA [14]	B 91.6	45.3	83.8	37.5	31.0	29.8	85.8	37.8	87.2	61.7	30.4	86.2	34.4	47.7	0.0	21.2	2.0	0.0	45.2	47.8
	L 91.5	44.5	83.9	36.5	31.2	28.1	86.1	41.0	87.1	62.0	33.1	86.3	29.2	40.3	0.0	19.8	2.0	0.0	44.6	47.2
AdaptSegNet + KRADA	B 73.7	26.0	79.6	21.4	23.7	27.5	81.9	32.9	74.9	52.4	14.3	78.6	26.1	32.0	0.0	19.9	0.0	1.0	37.0	39.1
	L 76.8	24.9	78.1	18.1	23.8	25.8	81.0	27.9	73.2	53.0	14.5	79.2	22.8	30.8	0.1	17.8	0.1	0.7	36.0	38.1
CLAN + KRADA	B 85.9	14.9	78.6	20.8	23.6	28.0	83.3	33.7	79.7	52.1	17.2	80.2	31.3	39.6	0.0	24.9	0.2	1.1	38.6	40.8
	L 85.1	15.2	78.6	20.4	23.6	28.2	83.0	31.1	78.7	53.1	15.7	79.3	31.5	37.8	0.0	24.7	0.1	1.0	38.2	40.4
FADA + KRADA	B 92.0	47.5	82.2	30.1	31.3	33.0	84.7	37.1	79.7	61.3	32.6	83.6	35.5	48.1	0.0	28.7	6.2	0.9	45.2	47.9
	L 91.2	42.4	82.2	30.2	31.7	33.8	84.4	36.7	79.9	61.2	32.2	83.1	34.5	44.0	0.0	30.6	6.2	1.0	44.7	47.3

Under the AdaptSegNet architecture, KRADA brings around +2.0% improvements in both mIoU and mIoU* as well as a significant gain in unknown-class IoU at the last and best epochs. CLAN + KRADA outperforms CLAN at the last epoch, whereas it obtains a little bit worse performance in mIoU and mIoU* than CLAN at the best epoch because it sacrifices the segmentation performance on known classes to achieve 1.1% (the highest) unknown-class IoU. Besides, we also observe that KRADA helps achieve a small variance throughout the training phase since the gaps of results between the last and best epochs become small after realizing KRADA on CLAN. Furthermore, FADA + KRADA boosts unknown-class IoU by 1.0% and obtains slight improvements on mIoU and mIoU* compared to FADA.

Overall, the results shown in Table 1 and Table 2 demonstrate that KRADA can enable CSDAS methods to identify unknown-class regions and promote a better overall adaptation by rejecting unknown-class regions and conducting the known-region-aware domain alignment. We also provide some qualitative segmentation results in Figure 4.

Ablation studies³: To retain as many source images as possible, we select the minority classes to

³For simplicity, we conduct ablation studies under the CLAN architecture where the training process is end-to-end instead of multiple training phases in FADA. Here we report the scores of the last epoch. Full results can be found in Appendix B.

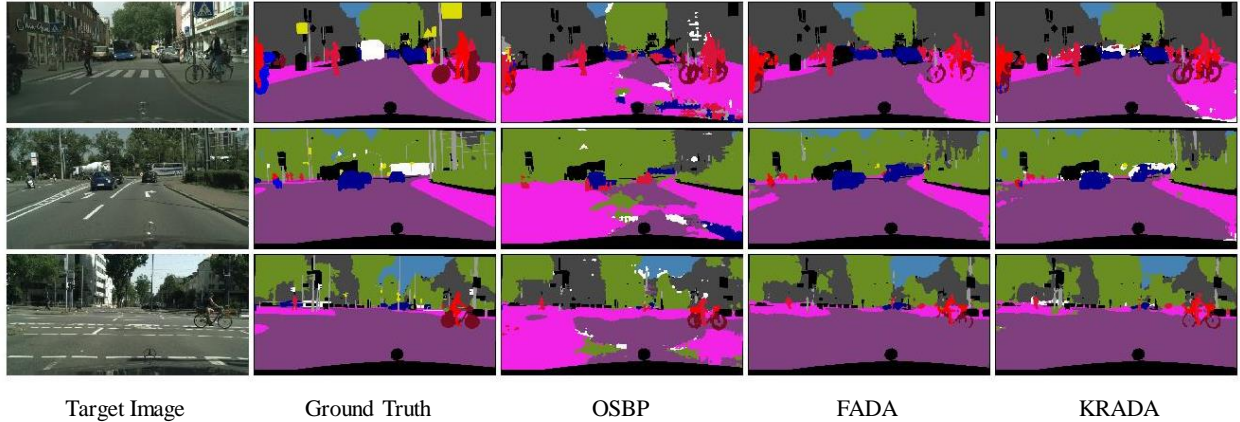


Figure 4: Qualitative results on SYNTHIA → Cityscapes. Each row is a target image in Cityscapes. From left to right, columns correspond to original images, ground truth, and segmentation results of OSBP, FADA, and a realization of KRADA, where the white area denotes the unknown-class region.

Table 3: Ablation study of varying the unknown class on GTA5 → Cityscapes.

Method	road	side.	build.	wall	pole	light	terrain	veg.	sky	person	rider	car	truck	bus	train	motor	bike	unk.	mIoU	mIoU*
CLAN [13]	53.8	17.8	59.9	17.9	16.5	16.2	8.2	82.2	29.4	79.4	51.3	4.3	19.2	6.7	0.0	15.6	3.3	0.0	26.8	28.3
CLAN + KRADA	34.7	14.1	67.3	18.3	20.1	17.5	9.9	81.0	29.6	77.9	53.0	5.3	22.2	7.3	0.0	15.6	8.4	21.2	28.0	28.4

construct the unknown class in the above experiments. Even though KRADA makes three CSDAS methods capable of detecting unknown regions, the unknown-class IoU values are not very large, especially for the GTA5 → Cityscape task in Table 2. This is because that the unknown class is a challenging class to segment due to the imbalance issue. To explore the effect of the composition of the unknown class, we conduct an extra ablation study. We choose car and light to form a new unknown class in GTA5 → Cityscape where the car is a majority class. The results are shown in Table 3. Compared to Table 2, there is a sharp overall decline in both mIoU and mIoU* since an easy class (car) is excluded from known classes. Comparatively, KRADA drastically increases the unknown-class IoU from 0.0% to more than 20.0% under the CLAN architecture.

To investigate the impact of the known-region map R^{kn} and the statistical measure used in the pseudo-label generation, we compare two variants of CLAN + KRADA on SYNTHIA → Cityscapes in Table 4. The performance of CLAN + KRADA w/o R^{kn} is worse than CLAN + KRADA, which confirms the effectiveness of R^{kn} and the necessity of rejection of unknown-class regions in target images for domain alignment. We further replace KL divergence with Kolmogorov metric as the criterion for pseudo-label generation, denoted as CLAN + KRADA with Ko. We can see that it achieves better performance in identifying the unknown class and obtains comparable performance in known classes. This indicates that the statistical metric to measure the distribution disparity is not fixed. We can adjust it to suit our needs, which proves the adjustability and flexibility of KRADA.

Real-world OSS task (COVID-19 infection segmentation in CT scans). To construct a COVID-19 task, we exploit the public datasets summarized in [36]. The source data consists of normal CT scans with lung annotations. Both target data and test data include COVID-19 cases and non-infected CT scans. Detailed data descriptions and data processes are introduced in Appendix B. To give a comprehensive comparison, we evaluate the proposed method from both pixel-level and instance-level aspects. The IoU values of lung and infection averaged among all test cases are reported in Table 5, denoted as Lung_IoU and Infection_IoU. We also provide four other metrics: Accuracy, Precision, Recall, and F1-score, commonly used in medical fields for instance-level evaluation.

Table 4: Results of ablation study on SYNTHIA → Cityscapes. “w/o” indicates without known-region map R^{kn} . “Ko” denotes Kolmogorov metric, instead of KL divergence, used as a criterion for pseudo-label generation.

Method	road	side.	build.	fence	pole	sign	veg.	sky	person	rider	car	motor	bike	unk.	mIoU	mIoU*
CLAN + KRADA w/o	73.9	37.1	77.5	0.1	21.5	2.0	78.6	76.8	47.2	16.9	80.3	13.0	25.3	0.8	39.4	42.3
CLAN + KRADA Ko	83.5	35.0	76.1	0.0	22.9	3.0	74.7	72.2	47.5	17.8	72.0	14.8	27.5	3.9	39.3	42.1
CLAN + KRADA	77.6	37.4	77.0	0.0	22.4	2.0	76.2	75.2	48.5	17.3	80.1	13.8	29.8	1.6	39.9	42.9

Table 5: Results on COVID-19 infection segmentation.

Method	Lung_IoU	Infection_IoU	Accuracy	Precision	Recall	F1-score
OSBP [8]	69.9	0.6	66.7	66.7	100.0	80.0
AdaptSegNet + KRADA	85.6	0.5	66.7	66.7	100.0	80.0
CLAN + KRADA	85.1	0.9	73.3	71.4	100.0	83.3
FADA + KRADA	86.7	2.1	86.7	83.3	100.0	90.9

Results on real-world OSS task. In Table 5, all these models achieve 100.0% recall, meaning that all infected cases are detected, which is desirable in medical image diagnosis. Specifically, OSBP gains a non-zero IoU in infection and the same instance-level performance as AdaptSegNet + KRADA, but it heavily sacrifices the segmentation accuracy of the lung. Compared with OSBP, CLAN + KRADA shows superior segmentation performance in both pixel-level and instance-level evaluations. Moreover, FADA + KRADA greatly outperforms OSBP and obtains the best results. Examples of segmentation results are provided in Figure 5.

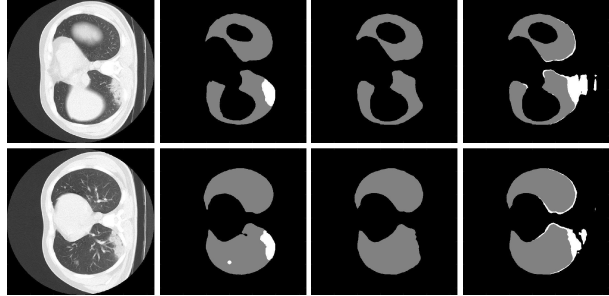


Figure 5: Examples of results on a COVID-19 task. From left to right: CT slice, Ground Truth, and the results of FADA and FADA + KRADA, where the brighter area is the infected area.

7 Conclusion

This paper is the first work to consider the semantic segmentation task in an open world, where test images have a different distribution from training images and contain unknown categories/classes. To address this new and challenging problem, we explore the inherent property of unknown classes and propose an end-to-end framework, KRADA, that performs known-region-aware domain alignment. KRADA is a generalized framework with no particular structure dependency and can be easily implemented on existing CSDAS methods, as demonstrated by three realizations of KRADA in our experiments. Experimental results validate that KRADA enables CSDAS methods to distinguish unknown-class pixels from known-class pixels and classify known-class pixels well.

References

- [1] Marius Cordts, Mohamed Omran, Sebastian Ramos, Timo Rehfeld, Markus Enzweiler, Rodrigo Benenson, Uwe Franke, Stefan Roth, and Bernt Schiele. The cityscapes dataset for semantic urban scene understanding. In *Proceedings of the IEEE Conference on Computer Vision and Pattern Recognition (CVPR)*, pages 3213–3223, 2016.

[2] Mennatullah Siam, Mostafa Gamal, Moemen Abdel-Razek, Senthil Yogamani, Martin Jagersand, and Hong Zhang. A comparative study of real-time semantic segmentation for autonomous driving. In *Proceedings of the IEEE Conference on Computer Vision and Pattern Recognition Workshops*, pages 587–597, 2018.

[3] Nathan Silberman, Derek Hoiem, Pushmeet Kohli, and Rob Fergus. Indoor segmentation and support inference from rgbd images. In *Proceedings of the European Conference on Computer Vision (ECCV)*, pages 746–760. Springer, 2012.

[4] Nima Tajbakhsh, Laura Jeyaseelan, Qian Li, Jeffrey N Chiang, Zhihao Wu, and Xiaowei Ding. Embracing imperfect datasets: A review of deep learning solutions for medical image segmentation. *Medical Image Analysis*, 63:101693, 2020.

[5] Alberto Garcia-Garcia, Sergio Orts-Escalano, Sergiu Oprea, Victor Villena-Martinez, and Jose Garcia-Rodriguez. A review on deep learning techniques applied to semantic segmentation. *arXiv preprint arXiv:1704.06857*, 2017.

[6] Jonathan Long, Evan Shelhamer, and Trevor Darrell. Fully convolutional networks for semantic segmentation. In *Proceedings of the IEEE Conference on Computer Vision and Pattern Recognition (CVPR)*, pages 3431–3440, 2015.

[7] Pau Panareda Busto and Juergen Gall. Open set domain adaptation. In *Proceedings of the IEEE International Conference on Computer Vision (ICCV)*, pages 754–763, 2017.

[8] Kuniaki Saito, Shohei Yamamoto, Yoshitaka Ushiku, and Tatsuya Harada. Open set domain adaptation by backpropagation. In *Proceedings of the European Conference on Computer Vision (ECCV)*, pages 153–168, 2018.

[9] German Ros, Laura Sellart, Joanna Materzynska, David Vazquez, and Antonio M Lopez. The synthia dataset: A large collection of synthetic images for semantic segmentation of urban scenes. In *Proceedings of the IEEE Conference on Computer Vision and Pattern Recognition (CVPR)*, pages 3234–3243, 2016.

[10] Judy Hoffman, Dequan Wang, Fisher Yu, and Trevor Darrell. Fcns in the wild: Pixel-level adversarial and constraint-based adaptation. *arXiv preprint arXiv:1612.02649*, 2016.

[11] Tuan-Hung Vu, Himalaya Jain, Maxime Bucher, Matthieu Cord, and Patrick Pérez. Advent: Adversarial entropy minimization for domain adaptation in semantic segmentation. In *Proceedings of the IEEE Conference on Computer Vision and Pattern Recognition (CVPR)*, pages 2517–2526, 2019.

[12] Yi-Hsuan Tsai, Wei-Chih Hung, Samuel Schulter, Kihyuk Sohn, Ming-Hsuan Yang, and Manmohan Chandraker. Learning to adapt structured output space for semantic segmentation. In *Proceedings of the IEEE Conference on Computer Vision and Pattern Recognition (CVPR)*, pages 7472–7481, 2018.

[13] Yawei Luo, Liang Zheng, Tao Guan, Junqing Yu, and Yi Yang. Taking a closer look at domain shift: Category-level adversaries for semantics consistent domain adaptation. In *Proceedings of the IEEE Conference on Computer Vision and Pattern Recognition (CVPR)*, pages 2507–2516, 2019.

[14] Haoran Wang, Tong Shen, Wei Zhang, Ling-Yu Duan, and Tao Mei. Classes matter: A fine-grained adversarial approach to cross-domain semantic segmentation. In *Proceedings of the European Conference on Computer Vision (ECCV)*, pages 642–659. Springer, 2020.

[15] Kuniaki Saito, Kohei Watanabe, Yoshitaka Ushiku, and Tatsuya Harada. Maximum classifier discrepancy for unsupervised domain adaptation. In *Proceedings of the IEEE Conference on Computer Vision and Pattern Recognition (CVPR)*, pages 3723–3732, 2018.

[16] Ke Mei, Chuang Zhu, Jiaqi Zou, and Shanghang Zhang. Instance adaptive self-training for unsupervised domain adaptation. *arXiv preprint arXiv:2008.12197*, 2020.

[17] Yang Zou, Zhiding Yu, Xiaofeng Liu, BVK Kumar, and Jinsong Wang. Confidence regularized self-training. In *Proceedings of the IEEE International Conference on Computer Vision (ICCV)*, pages 5982–5991, 2019.

[18] Qiming Zhang, Jing Zhang, Wei Liu, and Dacheng Tao. Category anchor-guided unsupervised domain adaptation for semantic segmentation. In *Advances in Neural Information Processing Systems (Neurips)*, pages 433–443, 2019.

[19] Guoliang Kang, Yunchao Wei, Yi Yang, Yueling Zhuang, and Alexander Hauptmann. Pixel-level cycle association: A new perspective for domain adaptive semantic segmentation. In *Advances in Neural Information Processing Systems (Neurips)*, 2020.

[20] Silvia Bucci, Mohammad Reza Loghmani, and Tatiana Tommasi. On the effectiveness of image rotation for open set domain adaptation. In *Proceedings of the European Conference on Computer Vision (ECCV)*, pages 422–438. Springer, 2020.

[21] Kai-Sheng Song. Goodness-of-fit tests based on kullback-leibler discrimination information. *IEEE Transactions on Information Theory*, 48(5):1103–1117, 2002.

[22] Alison L Gibbs and Francis Edward Su. On choosing and bounding probability metrics. *International statistical review*, 70(3):419–435, 2002.

[23] Abhijit Bendale and Terrance Boult. Towards open world recognition. In *Proceedings of the IEEE Conference on Computer Vision and Pattern Recognition (CVPR)*, pages 1893–1902, 2015.

[24] K J Joseph, Salman Khan, Fahad Shahbaz Khan, and Vineeth N Balasubramanian. Towards open world object detection. In *Proceedings of the IEEE Conference on Computer Vision and Pattern Recognition (CVPR)*, 2021.

[25] Jaedong Hwang, Seoung Wug Oh, Joon-Young Lee, and Bohyung Han. Exemplar-based open-set panoptic segmentation network. In *Proceedings of the IEEE Conference on Computer Vision and Pattern Recognition (CVPR)*, 2021.

[26] Zhiying Cui, Wu Longshi, and Ruixuan Wang. Open set semantic segmentation with statistical test and adaptive threshold. In *2020 IEEE International Conference on Multimedia and Expo (ICME)*, pages 1–6, 2020.

[27] Terrance E Boult, Steve Cruz, Akshay Raj Dhamija, M Gunther, James Henrydoss, and Walter J Scheirer. Learning and the unknown: Surveying steps toward open world recognition. In *Proceedings of the AAAI Conference on Artificial Intelligence (AAAI)*, pages 9801–9807, 2019.

[28] Marc Kéry and J Andrew Royle. *Applied Hierarchical Modeling in Ecology: Analysis of distribution, abundance and species richness in R and BUGS: Volume 1: Prelude and Static Models*. Academic Press, 2015.

[29] Oldrich Vasicek. A test for normality based on sample entropy. *Journal of the Royal Statistical Society: Series B (Methodological)*, 38(1):54–59, 1976.

[30] Yang Zou, Zhiding Yu, BVK Kumar, and Jinsong Wang. Unsupervised domain adaptation for semantic segmentation via class-balanced self-training. In *Proceedings of the European Conference on Computer Vision (ECCV)*, pages 289–305, 2018.

[31] Judy Hoffman, Eric Tzeng, Taesung Park, Jun-Yan Zhu, Phillip Isola, Kate Saenko, Alexei Efros, and Trevor Darrell. Cycada: Cycle-consistent adversarial domain adaptation. In *International Conference on Machine Learning (ICML)*, pages 1989–1998, 2018.

[32] Rui Gong, Wen Li, Yuhua Chen, and Luc Van Gool. Dlow: Domain flow for adaptation and generalization. In *Proceedings of the IEEE Conference on Computer Vision and Pattern Recognition (CVPR)*, pages 2477–2486, 2019.

[33] Yuhua Chen, Wen Li, Xiaoran Chen, and Luc Van Gool. Learning semantic segmentation from synthetic data: A geometrically guided input-output adaptation approach. In *Proceedings of the IEEE Conference on Computer Vision and Pattern Recognition (CVPR)*, pages 1841–1850, 2019.

[34] Stephan R Richter, Vibhav Vineet, Stefan Roth, and Vladlen Koltun. Playing for data: Ground truth from computer games. In *Proceedings of the European Conference on Computer Vision (ECCV)*, pages 102–118. Springer, 2016.

[35] Yadan Luo, Zijian Wang, Zi Huang, and Mahsa Baktashmotagh. Progressive graph learning for open-set domain adaptation. In *International Conference on Machine Learning (ICML)*, pages 6468–6478, 2020.

[36] Jun Ma, Yixin Wang, Xingle An, Cheng Ge, Ziqi Yu, Jianan Chen, Qiongjie Zhu, Guoqiang Dong, Jian He, Zhiqiang He, et al. Towards efficient covid-19 ct annotation: A benchmark for lung and infection segmentation. *arXiv preprint arXiv:2004.12537*, 2020.

[37] Hong Liu, Zhangjie Cao, Mingsheng Long, Jianmin Wang, and Qiang Yang. Separate to adapt: Open set domain adaptation via progressive separation. In *Proceedings of the IEEE Conference on Computer Vision and Pattern Recognition (CVPR)*, pages 2927–2936, 2019.

[38] Yingwei Pan, Ting Yao, Yehao Li, Chong-Wah Ngo, and Tao Mei. Exploring category-agnostic clusters for open-set domain adaptation. In *Proceedings of the IEEE Conference on Computer Vision and Pattern Recognition (CVPR)*, pages 13867–13875, 2020.

[39] Jogendra Nath Kundu, Naveen Venkat, Ambareesh Revanur, R Venkatesh Babu, et al. Towards inheritable models for open-set domain adaptation. In *Proceedings of the IEEE Conference on Computer Vision and Pattern Recognition (CVPR)*, pages 12376–12385, 2020.

[40] Zhen Fang, Jie Lu, Feng Liu, Junyu Xuan, and Guangquan Zhang. Open set domain adaptation: Theoretical bound and algorithm. *IEEE Transactions on Neural Networks and Learning Systems*, 2020.

[41] Li Zhong, Zhen Fang, Feng Liu, Bo Yuan, Guangquan Zhang, and Jie Lu. Bridging the theoretical bound and deep algorithms for open set domain adaptation. *arXiv preprint arXiv:2006.13022*, 2020.

[42] Qianyu Feng, Guoliang Kang, Hehe Fan, and Yi Yang. Attract or distract: Exploit the margin of open set. In *Proceedings of the IEEE International Conference on Computer Vision (ICCV)*, pages 7990–7999, 2019.

[43] Marco Toldo, Andrea Maracani, Umberto Michieli, and Pietro Zanuttigh. Unsupervised domain adaptation in semantic segmentation: a review. *Technologies*, 8(2):35, 2020.

[44] Yunsheng Li, Lu Yuan, and Nuno Vasconcelos. Bidirectional learning for domain adaptation of semantic segmentation. In *Proceedings of the IEEE Conference on Computer Vision and Pattern Recognition (CVPR)*, pages 6936–6945, 2019.

[45] Yi-Hsuan Tsai, Kihyuk Sohn, Samuel Schulter, and Manmohan Chandraker. Domain adaptation for structured output via discriminative patch representations. In *Proceedings of the IEEE International Conference on Computer Vision (ICCV)*, pages 1456–1465, 2019.

[46] Liang-Chieh Chen, George Papandreou, Iasonas Kokkinos, Kevin Murphy, and Alan L Yuille. Deeplab: Semantic image segmentation with deep convolutional nets, atrous convolution, and fully connected crfs. *IEEE transactions on pattern analysis and machine intelligence*, 40(4):834–848, 2017.

- [47] Kaiming He, Xiangyu Zhang, Shaoqing Ren, and Jian Sun. Deep residual learning for image recognition. In *Proceedings of the IEEE Conference on Computer Vision and Pattern Recognition (CVPR)*, pages 770–778, 2016.
- [48] Jia Deng, Wei Dong, Richard Socher, Li-Jia Li, Kai Li, and Li Fei-Fei. Imagenet: A large-scale hierarchical image database. In *Proceedings of the IEEE Conference on Computer Vision and Pattern Recognition (CVPR)*, pages 248–255. Ieee, 2009.
- [49] KJ Kiser, S Ahmed, SM Stieb, et al. Data from the thoracic volume and pleural effusion segmentations in diseased lungs for benchmarking chest ct processing pipelines. *The Cancer Imaging Archive*, 2020.
- [50] Hugo JWJ Aerts, Emmanuel Rios Velazquez, Ralph TH Leijenaar, Chintan Parmar, Patrick Grossmann, Sara Carvalho, Johan Bussink, René Monshouwer, Benjamin Haibe-Kains, Derek Rietveld, et al. Decoding tumour phenotype by noninvasive imaging using a quantitative radiomics approach. *Nature communications*, 5(1):1–9, 2014.
- [51] Kenneth Clark, Bruce Vendt, Kirk Smith, John Freymann, Justin Kirby, Paul Koppel, Stephen Moore, Stanley Phillips, David Maffitt, Michael Pringle, et al. The cancer imaging archive (tcia): maintaining and operating a public information repository. *Journal of digital imaging*, 26(6):1045–1057, 2013.
- [52] Ma Jun, Ge Cheng, Wang Yixin, An Xingle, Gao Jiantao, Yu Ziqi, Zhang Minqing, Liu Xin, Deng Xueyuan, Cao Shucheng, et al. Covid-19 ct lung and infection segmentation dataset. [Online]. Available: <https://doi.org/10.5281/zenodo.3757476>, 2020.
- [53] Dominik Müller, Iñaki Soto Rey, and Frank Kramer. Automated chest ct image segmentation of covid-19 lung infection based on 3d u-net. *arXiv preprint arXiv:2007.04774*, 2020.

A Related Works

In this section, we briefly review two kinds of domain adaptation settings related to open world semantic segmentation (OSS).

Unsupervised open set domain adaptation (UOSDA) is first proposed by Bustos *et al.* [7], where both source and target domain contain private and shared classes, but we only know shared labels. To relax the requirement of private source labels, Saito *et al.* [8] introduce a new concept of UOSDA setting where only target domain has private labels and propose Open Set Back-Propagation (OSBP), a novel adversarial training based method for an open set scenario. Later on, UOSDA methods follow this new and realistic setting and cope with it by a coarse-to-fine weighting mechanism [37], a self-supervised task [20], self-ensembling [38], or inheritable models [39]. Additionally, [40, 41] provide theoretical analysis for UOSDA and introduce open set difference, a special term that facilitates recognizing unknown target samples. Feng *et al.* [42] explicitly utilize the semantic margin of open set data to make the unknown class apart from the decision boundary and the known classes more separable. Luo *et al.* [35] propose a graph neural network with episodic training and achieve state-of-the-art performance. However, these existing UOSDA methods only focus on classification tasks, and most of them cannot be modified for semantic segmentation by simply convolutionalizing their classification architectures. For example, the state-of-the-art UOSDA method [35] requires source episodes containing each known class in a batch to construct a graph neural network. This requirement is hard to meet in segmentation tasks which demand a large memory to support dense computations. Therefore, modifying existing UOSDA methods for OSS is not usually feasible.

Closed set domain adaptation for semantic segmentation (CSDAS) has been extensively studied and developed maturely [43]. A predominant stream of CSDAS works is adversarial training (AT) based methods which minimize adversarial losses to align the distributions between the source and target domains at input level [31, 32], feature level [10, 11, 33, 14, 31], or output space level [13, 15, 12]. Recently, a series of approaches [30, 16, 17, 18] based on deep self-training (ST) has become an alternative research direction. These approaches generate pseudo-labels for target samples to provide extra supervision so that the network can be trained under the supervision of two domains. Zou *et al.* [30] propose a class-balanced self-training (CBST) framework to overcome the issue of imbalanced target pseudo-labels. To avoid overconfident wrong pseudo-labels, Zou *et al.* [17] further incorporate two types of confidence regularization to CBST. To generate high-quality pseudo-labels, Mei *et al.* [16] propose a instance adaptive selector to generate more accurate pseudo-labels. In addition, several works [44, 45] have been developed by combining AT and ST methods and presented a great potential. Despite the well-studied CSDAS methods, they cannot detect unknown classes and lead to negative transfer due to mismatched label sets. Therefore, current CSDAS methods are not applicable to an open world and cannot solve OSS tasks well.

Based on such well-studied CSDAS methods, we propose an end-to-end framework, KRADA, which can modify current CSDAS segmentation methods and adapt them for OSS tasks.

B Experiment Setup

B.1 Experiments on Two Synthetic OSS Tasks

Data description: For the task SYNTHIA \rightarrow Cityscapes, SYNTHIA originally includes 9,400 synthetic images and has 16 common classes with Cityscapes. These three classes (wall, light, and bus) are selected to form the unknown class, and we discard those images containing either of the three classes. The remaining data in SYNTHIA contain 750 images, and there are 13 shared known classes in this task. For the task GTA5 \rightarrow Cityscapes, GTA5 initially contains 24,966 images rendered from the GTA5 game engine and has the same 19 category annotations as Cityscapes. Similarly, we choose two classes (fence and sign) as the unknown class and only retain the images which do not contain the unknown class. The remaining images in GTA5 include 17 categories and 2,277 images. Cityscapes is a real-world dataset consisting of a training set with 2,957 images and a validation set with 500 images. We divide the Cityscapes training set into training splits of 2,500 images for training and evaluation splits of 457 images for hyperparameter selection. The results on

Table 6: Full results of varying the unknown class on GTA5 → Cityscapes. “B” denotes the best score during training, while “L” denotes the last score at the end of training.

Method	road	side.	build.	wall	pole	light	terrain	veg.	sky	person	rider	car	truck	bus	train	motor	bike	unk.	mIoU	mIoU*
CLAN [13]	B 58.1	18.4	61.0	19.2	17.8	19.3	11.0	81.8	29.5	78.5	52.0	7.2	20.1	8.0	0.0	18.6	5.0	0.0	28.1	29.7
	L 53.8	17.8	59.9	17.9	16.5	16.2	8.2	82.2	29.4	79.4	51.3	4.3	19.2	6.7	0.0	15.6	3.3	0.0	26.8	28.3
CLAN + KRADA	B 44.7	13.1	73.8	18.1	19.6	17.8	10.8	80.2	30.0	73.1	51.9	3.8	23.4	15.7	0.0	16.1	5.9	27.8	29.2	29.3
	L 34.7	14.1	67.3	18.3	20.1	17.5	9.9	81.0	29.6	77.9	53.0	5.3	22.2	7.3	0.0	15.6	8.4	21.2	28.0	28.4

Table 7: Full results of ablation study on SYNTHIA → Cityscapes. “w/o” indicates without known-region map R^{kn} . “Ko” denotes Kolmogorov metric, instead of KL divergence, used as a criterion for pseudo-label generation. “B” denotes the best score during training, while “L” denotes the last score at the end of training.

Method		road	side.	build.	fence	pole	sign	veg.	sky	person	rider	car	motor	bike	unk.		mIoU	mIoU*
CLAN + KRADA	w/o	B 77.1	37.0	77.6	0.0	22.6	2.8	77.4	78.4	48.9	18.6	81.6	13.5	30.0	1.3	40.5	43.5	
		L 73.9	37.1	77.5	0.1	21.5	2.0	78.6	76.8	47.2	16.9	80.3	13.0	25.3	0.8	39.4	42.3	
CLAN + KRADA	Ko	B 81.6	36.4	77.1	0.0	22.4	2.1	76.5	76.7	48.2	17.9	71.2	14.0	30.9	4.2	39.9	42.7	
		L 83.5	35.0	76.1	0.0	22.9	3.0	74.7	72.2	47.5	17.8	72.0	14.8	27.5	3.9	39.3	42.1	
CLAN + KRADA		B 80.6	36.8	77.8	0.0	24.6	2.4	76.7	77.1	49.3	18.1	81.7	14.3	30.7	2.1	40.9	43.9	
		L 77.6	37.4	77.0	0.0	22.4	2.0	76.2	75.2	48.5	17.3	80.1	13.8	29.8	1.6	39.9	42.9	

the Cityscapes validation set are reported for performance comparison.

Implementation details: For a fair comparison, we adopt the Deeplab-V2 [46] framework with ResNet-101 [47] pretrained on ImageNet [48] as the segmentation base network. We implement KRADA on three CSDAS methods: AdaptSegNet [12], CLAN [13], and FADA [14]. For each CSDAS method, we additionally duplicate a last convolution classification module as C^* which is arranged in parallel with the original classifier C after the feature extractor. C^* is identical as C expect for the last layer with channel number $\{K\}$ to output the predicted score map over known classes. Regarding the pseudo-label hyperparameters in KRADA, α is empirically defined as 0.1 for balancing the known classes and unknown classes. We adjust the value of δ from the mean minimum of KL divergence in a step-wise incremented manner to find the optimum. Eventually, for SYNTHIA → Cityscapes task, δ and α are set to 1.0 and 0.1 in AdaptSegNet + KRADA and CLAN + KRADA, while they are set to 0.02 and 0.1 in FADA + KRADA¹. For GTA5 → Cityscapes task, δ and α are set to 1.2 and 0.1 in AdaptSegNet + KRADA and CLAN + KRADA, while they are set to 0.025 and 0.3 in FADA + KRADA. Other experimental settings such as discriminator structure, optimization policy, and hyperparameters in three modified models are almost the same as those described in the original papers. All the models are implemented using Python 3.6 and Pytorch 1.7 on a TITAN Tesla V100 GPU.

Results: We report the full results of ablation studies in Table 6 and Table 7. In Table 6, CLAN + KRADA outperforms CLAN with a significant increase in unknown-class IoU from 0.0% to 21.2% at the last epoch, while it achieves the best unknown-class IoU (27.8%) at the expense of a slight drop in segmenting known classes at the best epoch. Moreover, we can observe the full results in Table 7 to draw consistent conclusions about the known-region map and the statistical measurement, respectively. Furthermore, to justify the necessity of considering the distributional discrepancy, we remove the discriminator which conducts the domain alignment and only introduce pseudo-labels into the network training. This model is denoted as Source-only + PL, and the results are shown in 8. After introducing the unknown-class pseudo-labels, Source-only + PL gains the ability to detect the unknown-class regions compared to Source-only. However, its segmentation performance on known classes is still worse as a result of the distribution shift.

B.2 Experiments on COVID-19 Infection Segmentation in CT Scans

We describe the details of our data used in the COVID-19 infection segmentation task. More specifically, we exploit the public datasets summarized in [36] to construct a real-world OSS task. Source data includes 30

¹FADA utilizes softmax temperature to output soft probability distribution, so δ becomes small.

Table 8: Further results on SYNTHIA → Cityscapes. “B” denotes the best score during training, while “L” denotes the last score at the end of training.

Method	road	side.	build.	fence	pole	sign	veg.	sky	person	rider	car	motor	bike	unk.	mIoU	mIoU*
Soure-only	B 39.9	19.2	65.4	0.0	22.4	2.0	63.8	70.2	47.8	14.0	47.9	7.5	26.2	0.0	30.4	32.8
	L 34.5	18.0	61.7	0.0	20.9	2.0	60.1	67.8	48.0	15.7	46.5	8.4	26.2	0.0	29.3	31.5
Soure-only + PL	B 33.2	24.7	70.7	0.1	23.7	4.8	66.8	68.0	46.0	15.9	40.1	11.2	36.4	1.8	31.7	34.0
	L 23.4	26.2	71.7	0.1	25.2	4.2	62.6	65.0	47.4	15.6	40.7	9.3	33.8	1.6	30.5	32.7
OSBP [8]	B 31.7	17.4	67.5	0.0	20.3	0.4	63.0	71.0	33.3	11.7	60.8	7.7	26.2	1.7	29.5	31.6
	L 28.7	16.3	66.6	0.1	19.5	0.6	59.0	72.7	28.9	7.0	50.2	3.2	23.9	2.0	27.0	29.0
FADA [14]	B 84.5	39.0	79.0	0.0	27.2	1.4	83.0	73.6	38.3	13.3	75.6	5.1	38.6	0.0	39.9	43.0
	L 82.6	37.5	79.0	0.0	25.8	1.8	82.9	74.8	37.7	12.9	76.3	6.6	35.0	0.0	39.5	42.5
FADA + KRADA	B 85.0	42.2	79.4	0.0	26.5	1.4	82.1	73.9	46.0	14.8	78.1	10.2	42.1	4.0	41.8	44.7
	L 82.2	39.4	79.2	0.0	29.0	1.5	82.1	75.9	44.9	13.9	78.5	8.9	38.5	3.3	41.2	44.2

CT scans which are randomly selected from NSCLC left and right lung segmentation dataset [49, 50, 51] (with CC BY-NC license). Target data consists of 20 COVID-19 CT scans and 10 non-infected CT scans. More specifically, COVID-19 CT scans are publicly available [52] (with CC BY-NC-SA license), and each case has the annotations of the left lung, right lung, and infection. Non-infected CT scans are randomly selected from StructSeg lung organ segmentation ², and we only use their left lung and right lung annotations. We divide the target data into two parts for training and testing, and each part includes 10 COVID-19 cases and 5 non-infected CT scans. Following [36], we adjust each CT scan to lung window [-1250, 250] and then normalize it to [0,255] for pre-processing. We slice each CT volume into 2D slices and perform the same data augmentation as [53]. In this task, the pseudo-label hyperparameters δ and α are set to 0.3 and 0.01 in AdaptSegNet + KRADA and CLAN + KRADA, while they are set to 0.02 and 0.1 in FADA + KRADA. Other experimental setups are similar to the above two synthetic tasks.

²MICCAI 2019 StructSeg: <https://structseg2019.grand-challenge.org>